Journal of Molecular Liquids 342 (2021) 117544

Contents lists available at ScienceDirect

Journal of Molecular Liquids

journal homepage: www.elsevier.com/locate/molliq

Molecular level interpretation of excess infrared spectroscopy

Maciej Śmiechowski

Department of Physical Chemistry, Faculty of Chemistry, Gdańsk University of Technology, Narutowicza 11/12, 80-233 Gdańsk, Poland

ARTICLE INFO

Article history:
Received 28 May 2021
Revised 6 September 2021
Accepted 9 September 2021
Available online 16 September 2021

Keywords:
Dimethyl sulfoxide
γ-butyrolactone
Ab initio molecular dynamics
Excess infrared spectroscopy
Infrared difference spectroscopy

ABSTRACT

Infrared (IR) spectroscopy is an invaluable tool in studying intermolecular interactions in solvent mixtures. The deviation of the IR spectrum of a mixture from the spectra of its pure components is a sensitive measure of the non-ideality of solutions and the modulation of intermolecular interactions introduced by mutual influence of the components. Excess IR spectroscopy, based on the established notion of excess thermodynamic functions, provides a well-defined picture of such deviation. On the other hand, the difference spectra method strives to obtain so-called affected spectra by numerically removing the bulk component contribution until the IR spectrum of the spectrally affected component is isolated. Although tremendously useful, excess IR spectroscopy remains poorly studied from a computational point of view. Based on ab initio molecular dynamics (AIMD) simulations, IR spectra of a dimethyl sulfoxide (DMSO)–γ-butyrolactone (GBL) liquid mixture are obtained here from first principles, without resorting to experimental input. Using dipolar decomposition techniques, the excess IR spectrum is further analyzed by rigorously separating the contributions from the modulation of the intra- and intermolecular parts of the spectra of both components and the mutual interaction spectrum. It is found that while the intramolecular part of excess IR spectrum is a good predictor of its overall shape, the intermolecular parts are crucial for elucidation of the band shifts and fine details of the IR spectrum of the mixture. Furthermore, the affected IR spectrum is obtained for both components by applying the spectral similarity method. The exact relationship between the affected and excess IR spectrum is derived and the latter is discovered as the predictor of the band shifts in the affected spectrum. Owing to a reduced cancellation effect of intermolecular contributions, the affected spectrum is a physically justified counterpart of the excess IR spectrum, providing a complementary view of the interactions in the mixture.

1. Introduction

Infrared (IR) spectroscopy is a long-established and indispensable method in the studies of molecular liquids and their mixtures [1–4]. To date, it continues to deliver a detailed picture of intermolecular interactions in mixed solvent systems [5–11]. Notorious troubles in the interpretation of the observed spectral changes in liquid mixtures can be circumvented by applying the quantitative version of the difference spectra method that allows to obtain the so-called affected spectrum of a system component by numerically removing the bulk component contribution with the aim of isolation of the IR spectrum of the spectrally affected part only [12–14]. The applicability of the method is particularly wide [15] and the combination with the chemometric procedures of subtraction factors determination [16,17] makes it amenable to more complex spectral scenarios.

For two-component systems, the notion of excess thermodynamic functions is well-established in physical chemistry and chemical physics [18]. Extending this approach to IR spectra as observables, excess IR spectroscopy studies deviations of the IR spectrum of a mixture from the ideal, strictly additive spectrum of its components, combining the sensitivity of excess functions to changes in thermodynamic properties with the responsiveness of the IR spectra to fluctuating intermolecular interactions in the system [19–26]. As already noted before [21], the two-state (i.e., affected vs bulk) model as assumed by the affected spectra method and the excess IR spectrum of the mixture are mutually correspondent.

From the computational perspective, ab initio molecular dynamics (AIMD) that combines quantum mechanical treatment of the electron density with the classical mechanics laws for the nuclear motion [27] provides a most accurate account of the physical and thermodynamic properties of complicated liquids [28,29]. For more than 20 years, AIMD has been the state of the art in liquid water simulations [30]. However, due to the demanding nature of AIMD simulations when it comes to computing power resources, the investigations of molecular solvents and other liquid systems, e.g., ionic liquids with this method are a novel and emerging area of computational studies [31–38]. Applying the maximally

E-mail address: maciej.smiechowski@pg.edu.pl

https://doi.org/10.1016/j.molliq.2021.117544
0167-7322/

localized Wannier functions (MLWF) formalism in AIMD simulations [39]—or its alternatives such as the Voronoi tessellation of the electron density of the system [40]—an unambiguous partitioning of the total dipole moment into molecular dipole moments is feasible in the liquid phase [41]. They can be further used in obtaining separate solute and solvent IR spectra based entirely on first principles [42–44]. In isotropic liquids, this dipole partitioning leads, inter alia, to clear separation of the intra- and intermolecular contributions to the IR spectrum [35,37]. This led us to suspect that a further generalization of this approach to liquid mixtures can help in elucidating the different mechanisms underlying the excess IR spectra of such systems.

Based on our recent AIMD investigations of liquid dimethyl sulfoxide (DMSO) [35] and γ-butyrolactone (GBL) [36,37], in this contribution we analyze in detail the IR spectra of their equimolar mixture as a proof of concept of the excess IR spectra decomposition based on molecular dipoles availability in our simulations. This particular system is characterized by moderate deviations from ideality that are most pronounced around the equimolar composition [45]. The DMSO–GBL mixture finds important applications in perovskite solar cells synthesis [46–48]. Its IR spectra are obtained here entirely from first principles, without resorting to experimental input. Using dipolar decomposition techniques, the excess IR spectrum is analyzed by rigorously separating the intra- and intermolecular contributions acting both within each component, as well as arising due to mutual interactions. This novel analysis method can help unravel the numerous phenomena that underlie the features observed in the experimentally determined excess IR spectra.

2. Theory

2.1. Infrared spectra from linear response theory

In linear response theory, the IR spectrum of a system in frequency space ω—expressed as linear absorption coefficient on the usual decadic logarithm scale—is obtained as a Fourier transform (FT) of the time correlation function (TCF) of the total dipole moment time derivative [49–51],

$$\alpha(\omega)\times n(\omega) = \frac{1}{6\ln(10)\epsilon_0 k_B TVc}\operatorname{sinc}^{-2}(\omega\delta t/2) \times \int_{-\infty}^{\infty} \mathrm{d}t\, \mathrm{e}^{-i\omega t}\left\langle \dot{\boldsymbol{M}}(t)\dot{\boldsymbol{M}}(0)\right\rangle, \quad (1)$$

where $\langle\ldots\rangle$ denotes the ensemble average at temperature T and volume V, while ϵ_0, k_B and c fundamental constants have the usual meaning. In the absence of true dipolar velocities (e.g., when using the MLWF formalism that provides static orbital centers), $\dot{\boldsymbol{M}}$ values must be approximated by finite differences, $\dot{\boldsymbol{M}} \approx \delta\boldsymbol{M}/\delta t$, where δt is the time step of the dipole moments trajectory. The $\operatorname{sinc}^{-2}(\omega\delta t/2)$ factor corrects for this time discretization [52]. While only the intensity function, $\alpha(\omega)\times n(\omega)$, is obtained in this manner, the components of the complex dielectric function, $\epsilon_r(\omega) = \epsilon\prime_r(\omega) + i\epsilon\prime\prime_r(\omega)$, obey the Kramers–Kronig relations. Since $\alpha(\omega)$ and $n(\omega)$ can be readily obtained from the parts of the complex dielectric function, numerical Kramers–Kronig transform can be used to remove the refractive index dispersion effects in the obtained IR intensity spectrum [43,52].

2.2. Excess infrared spectroscopy and infrared difference spectroscopy

Based on the well-established notion of excess functions in chemical thermodynamics [18], excess IR spectroscopy originates in defining the frequency-dependent excess molar absorptivity of a two-component system as [19–21,23],

$$\varepsilon^{\mathrm{E}} = \frac{A}{(c_1+c_2)d} - \left(x_1\varepsilon_1^* + x_2\varepsilon_2^*\right), \quad (2)$$

where A is the absorbance, d is the optical path length, c_1 and c_2 are the molarities of components 1 and 2 in the mixture, x_1 and x_2 are the respective mole fractions, while ε_1^* and ε_2^* are the molar absorptivities of the pure components.

We now introduce the linear absorption coefficient of the mixture, $\alpha_m = A/d$, as well as the linear absorption coefficients of the pure components, $\alpha_i^* = \varepsilon_i^* c_i^*$, where c_i^* is the molarity of component i in the pure state. Multiplying Eq. (2) by (c_1+c_2) and noticing that $x_i(c_1+c_2) = c_i$, we finally obtain the working definition of the excess linear absorption coefficient as,

$$\alpha^{\mathrm{E}} = \alpha_m - \left(c_1^r\alpha_1^* + c_2^r\alpha_2^*\right), \quad (3)$$

where $c_i^r = c_i/c_i^*$ is the relative concentration of component i in the mixture with respect to the pure state.

The excess molar absorptivities or absorption coefficients thus defined are not physical observable quantities, since excess spectra may contain both positive and negative features. However, the sign of excess IR spectrum may provide useful information concerning molecular interactions in the mixture, as well as indicate the direction of deviations from ideality [20]. Whenever the physically sound spectra are desirable, the difference spectra method may be used to isolate the IR spectrum of one component of the solution (i.e., solvent) affected by the other component (i.e., solute), assuming the rest of the solvent is present in the bulk (i.e., pure) state. The numerical procedure leading to the extraction of such spectrum was described in detail [12–14]. In essence, it requires the subtraction of the solvent IR spectrum from the solution spectrum in such proportion that a physically justified spectrum of the affected solvent is obtained. In practice, either band fitting approach [13,14] or chemometric procedures [16,17] may be used for this purpose. This analysis methodology is well attested for solvent mixtures in particular [53,5,6,9].

Following Stangret's approach [13,14], we divide each component in the mixture into the *bulk* (i.e., identical to the pure component) and *affected* (i.e., spectrally changed due to the interactions with the other component) contributions. However, since the solute–solvent distinction is often not justified in a mixture far from dilute conditions, we abandon the previous notion that the bulk vs affected partitioning pertains to *solvent* only and instead demand that $c_i = c_i^a + c_i^b$ holds for both components, where c_i^a and c_i^b are molarities of the affected and bulk component i, respectively. The principle of the additivity of absorption implies that,

$$\varepsilon_m(c_1+c_2) = \varepsilon_1^a c_1^a + \varepsilon_1^* c_1^b + \varepsilon_2^a c_2^a + \varepsilon_2^* c_2^b, \quad (4)$$

where $\varepsilon_m = \alpha_m/(c_1+c_2)$, ε_i^a is the molar absorptivity of the affected component i and the molar absorptivity of the bulk component is by definition identical to that of the pure substance.

Introducing the linear absorption coefficient of the affected part of the solution, $\alpha^{\mathrm{A}} = \varepsilon_1^a c_1^a + \varepsilon_2^a c_2^a$, and rewriting all molar absorptivities as linear absorption coefficients as above, we obtain,

$$\alpha^{\mathrm{A}} = \alpha_m - \left(\frac{c_1^b}{c_1^*}\alpha_1^* + \frac{c_2^b}{c_2^*}\alpha_2^*\right). \quad (5)$$

If we now introduce the fraction of the affected solvent, $c_i^a = k_i c_i$ and $c_i^b = (1-k_i)c_i$, we may rewrite Eq. (5) so that it resembles Eq. (3) as,

$$\alpha^{\mathrm{A}} = \alpha_m - \left[(1-k_1)c_1^r\alpha_1^* + (1-k_2)c_2^r\alpha_2^*\right]. \quad (6)$$

Comparing Eqs. (3) and (6), we see that the excess and affected IR spectra are directly related via,

$$\alpha^{\mathrm{A}} = \alpha^{\mathrm{E}} + k_1 c_1^r \alpha_1^* + k_2 c_2^r \alpha_2^*, \tag{7}$$

so that from the numerical standpoint the only difference between the two is the "incomplete" subtraction of the linear absorption coefficients of the pure components in α^{A}. We note here that similar connection between the two spectra was explored previously [21]. However, in contrast to the former approach, we do not discriminate between the solvent and solute in the mixture, treating both substances on equal terms. Moreover, we do not demand a strict two-state model, i.e., the molar absorptivities ε_i^q are not necessarily constant with mixture composition, reflecting the possibly fluctuating nature of the intermolecular complexes formed by the two substances in varying concentration regimes [9].

2.3. Molecular decomposition of excess infrared spectra

The previously proposed decomposition schemes for molecular dipoles allow for strict separation of the intra- and intermolecular contributions to the IR spectrum [43,42,54]. The total dipole moment in Eq. 1 can be formally decomposed into molecular dipole moments, so that $\dot{\boldsymbol{M}} = \sum_{i=1}^{N} \dot{\boldsymbol{\mu}}_i$. Accordingly, the TCF from Eq. (1) can be rewritten as,

$$\begin{aligned} \left\langle \dot{\boldsymbol{M}}(t)\dot{\boldsymbol{M}}(0) \right\rangle &= \left\langle \sum_{i=1}^{N} \dot{\boldsymbol{\mu}}_i(t) \sum_{i=1}^{N} \dot{\boldsymbol{\mu}}_i(0) \right\rangle \\ &= \sum_{i=1}^{N} \left\langle \dot{\boldsymbol{\mu}}_i(t)\, \dot{\boldsymbol{\mu}}_i(0) \right\rangle + \sum_{i=1}^{N} \sum_{j \neq i} \left\langle \dot{\boldsymbol{\mu}}_j(t)\, \dot{\boldsymbol{\mu}}_i(0) \right\rangle, \end{aligned} \tag{8}$$

and the IR spectrum can consequently be interpreted as,

$$\begin{aligned} \alpha^*(\omega) &= C(\omega) \int_{-\infty}^{\infty} \mathrm{d}t\, \mathrm{e}^{-i\omega t} \left[\sum_{i=1}^{N} \left\langle \dot{\boldsymbol{\mu}}_i(t)\, \dot{\boldsymbol{\mu}}_i(0) \right\rangle + \sum_{i=1}^{N} \sum_{j \neq i} \left\langle \dot{\boldsymbol{\mu}}_j(t)\, \dot{\boldsymbol{\mu}}_i(0) \right\rangle \right] \\ &= \alpha^{\circ}(\omega) + \alpha^{\times}(\omega), \end{aligned} \tag{9}$$

where by $C(\omega)$ we denote the entire frequency-dependent prefactor in Eq. (1). The equation above provides explicit definitions of the "self" and "cross" (i.e., intra- and intermolecular) terms in the IR spectrum of a pure liquid. We explored its ramifications for the interpretation of IR spectra of the pure solvents forming the system studied in this work previously [37,35].

For a two-component system, the decomposition of the total dipole moment into molecular contributions proceeds as,

$$\dot{\boldsymbol{M}} = \sum_{i=1}^{N_1} \dot{\boldsymbol{\mu}}_{i,1} + \sum_{i=1}^{N_2} \dot{\boldsymbol{\mu}}_{i,2},$$

and the TCF from Eq. (1) becomes,

$$\begin{aligned} \left\langle \dot{\boldsymbol{M}}(t)\dot{\boldsymbol{M}}(0) \right\rangle &= \left\langle \left(\sum_{i=1}^{N_1} \dot{\boldsymbol{\mu}}_{i,1}(t) + \sum_{i=1}^{N_2} \dot{\boldsymbol{\mu}}_{i,2}(t) \right) \left(\sum_{i=1}^{N_1} \dot{\boldsymbol{\mu}}_{i,1}(0) + \sum_{i=1}^{N_2} \dot{\boldsymbol{\mu}}_{i,2}(0) \right) \right\rangle \\ &= \sum_{i=1}^{N_1} \left\langle \dot{\boldsymbol{\mu}}_{i,1}(t)\, \dot{\boldsymbol{\mu}}_{i,1}(0) \right\rangle + \sum_{i=1}^{N_1} \sum_{j \neq i} \left\langle \dot{\boldsymbol{\mu}}_{j,1}(t)\, \dot{\boldsymbol{\mu}}_{i,1}(0) \right\rangle \\ &\quad + \sum_{i=1}^{N_2} \left\langle \dot{\boldsymbol{\mu}}_{i,2}(t)\, \dot{\boldsymbol{\mu}}_{i,2}(0) \right\rangle + \sum_{i=1}^{N_2} \sum_{j \neq i} \left\langle \dot{\boldsymbol{\mu}}_{j,2}(t)\, \dot{\boldsymbol{\mu}}_{i,2}(0) \right\rangle \\ &\quad + 2 \sum_{j=1}^{N_2} \sum_{i=1}^{N_1} \left\langle \dot{\boldsymbol{\mu}}_{j,2}(t)\, \dot{\boldsymbol{\mu}}_{i,1}(0) \right\rangle, \end{aligned} \tag{11}$$

allowing for an assumption-free division of the IR spectrum of the system into,

$$\alpha_m(\omega) = \alpha_1^{\circ}(\omega) + \alpha_1^{\times}(\omega) + \alpha_2^{\circ}(\omega) + \alpha_2^{\times}(\omega) + \alpha_{12}^{\times}(\omega),$$

i.e., into the intramolecular terms α_i°, the intermolecular terms *within the component* $\alpha_i^{\times}$ and the intermolecular *cross-component* term $\alpha_{12}^{\times}$.

Using the novel expression for the linear absorption coefficient of the mixture, Eq. (12), and the corresponding decomposition of the linear absorption coefficient of a pure liquid, Eq. (9), we may finally rewrite—dropping the frequency dependence of α for clarity—the definition of the excess linear absorption coefficient of a two-component system in terms of intra- and intermolecular contributions as,

$$\begin{aligned} \alpha^{\mathrm{E}} &= \alpha_1^{\circ} + \alpha_1^{\times} + \alpha_2^{\circ} + \alpha_2^{\times} + \alpha_{12}^{\times} - \left[c_1^r \left(\alpha_1^{\circ,*} + \alpha_1^{\times,*} \right) + c_2^r \left(\alpha_2^{\circ,*} + \alpha_2^{\times,*} \right) \right] \\ &= \left(\alpha_1^{\circ} - c_1^r \alpha_1^{\circ,*} \right) + \left(\alpha_1^{\times} - c_1^r \alpha_1^{\times,*} \right) + \left(\alpha_2^{\circ} - c_2^r \alpha_2^{\circ,*} \right) + \left(\alpha_2^{\times} - c_2^r \alpha_2^{\times,*} \right) + \alpha_{12}^{\times} \\ &= \Delta\alpha_1^{\circ} + \Delta\alpha_1^{\times} + \Delta\alpha_2^{\circ} + \Delta\alpha_2^{\times} + \alpha_{12}^{\times}, \end{aligned} \tag{13}$$

thus rigorously decomposing the excess IR spectrum into the change of the intramolecular part of the IR spectrum with respect to the pure solvent, $\Delta\alpha_i^{\circ}$, the respective change of the intermolecular part of the spectrum, $\Delta\alpha_i^{\times}$, and the cross-component term specific to the mixture, $\alpha_{12}^{\times}$.

Note that in the light of the connection between the excess and affected IR spectrum, Eq. (7), the latter can be similarly expressed as,

$$\alpha^{\mathrm{A}} = \Delta\prime\alpha_1^{\circ} + \Delta\prime\alpha_1^{\times} + \Delta\prime\alpha_2^{\circ} + \Delta\prime\alpha_2^{\times} + \alpha_{12}^{\times},$$

where the $\Delta\prime\alpha$ terms differ from the respective $\Delta\alpha$ terms only by the presence of the affected solvent fraction k.

3. Computational methods

AIMD simulations of pure liquid DMSO and GBL were reported previously [35–37]. Here, an equimolar mixture of the two solvents was simulated using the same protocol, as briefly summarized below. The studied system was composed of 17 molecules of each DMSO (1) and GBL (2) and was contained in a cubic supercell with edge length reproducing the experimental density of such mixture at 298.15 K (1108 kg m^{-3} [45]), so that $L \approx 16.114$ Å. The starting configuration was generated using PACKMOL [55]. Periodic boundary conditions were imposed throughout.

All simulations were carried out using the CP2K suite (v. 2.7) [56,57], in particular its QUICKSTEP electronic structure module based on DFT [58]. We used the standard BLYP functional [59,60] together with the DFT-D3 empirical dispersion correction [61] that accounts better for dispersion interactions in condensed phases. The TZV2P basis set was employed for atomic orbitals, while the cutoff for the auxiliary plane wave expansion of the electron density was set to 500 Ry. Only valence electrons were treated explicitly, while core electrons were approximated by GTH pseudo potentials [62]. The cutoff for the D3 correction was set to 18 Å.

The system was first equilibrated in the canonical (*NVT*) ensemble for 25 ps with temperature stabilization ensured by massive Nosé–Hoover chain thermostatting [63]. The time step in all simulations was set to 0.5 fs. We used an elevated temperature, specifically 360 K, in order to mimic liquid dynamics in standard conditions (298.15 K). Such empirical temperature rescaling is routinely applied to account for the temperature underestimation that is associated with DFT-based simulations of the liquid state [64,65] that results in the so-called "glassy dynamics" of the system. Detailed investigations of liquid water revealed that this "glassy" state manifests itself by a dramatically increased melting point [66] and by significantly retarded molecular mobility that results

in the calculated self-diffusion coefficient of the liquid being even an order of magnitude smaller than the experimental value [67,64,65]. The chosen simulation temperature accurately reproduced liquid DMSO and GBL mobility at standard conditions [35,36]. In the Supplementary Material, we show by comparison with experimental self-diffusion coefficients [68,69] that this is also the case for the DMSO–GBL mixture studied in this work (see Fig. S1 with the accompanying discussion).

After the equilibration, the canonical simulation was continued and 32 statistically independent initial conditions separated by 5 ps were sampled from it in order to initialize microcanonical (*NVE*) trajectories with 20 ps length each. During the latter runs, the centers of maximally localized Wannier functions were computed every 4 trajectory steps (2 fs) and further used to obtain molecular dipole moments. All reported observables were averaged over the 32 *NVE* trajectories in order to obtain proper canonical averages [70]. The aggregated simulation time of 640 ps provides adequate sampling for the convergence of TCFs, particularly the cross-correlation terms, as discussed below.

IR spectra were calculated based on the obtained molecular dipole moments according to the equations presented in Section 2.3. All spectra were smoothed for presentation by passing through a Gaussian filter with 5 cm^{-1} width. Numerical Kramers–Kronig transform was used to remove the refractive index dispersion influence on the IR spectra [52], using the average of the experimental refractive indices of DMSO and GBL, $n_D = 1.456$ [36,71].

4. Results and discussion

The nature and extent of the intermolecular contributions in liquid DMSO and GBL were studied previously [35,37], but we summarize the most important results here to set the stage for the following decomposition of the IR spectrum of the DMSO–GBL system. As seen in Fig. 1, in both liquids there is a non-negligible contribution of the $\alpha^{\times}(\tilde{\nu})$ term, which is apparently responsible for 20–30% of the total IR intensity across the shown spectral range. The intermolecular contribution in DMSO and GBL is mostly positive and no major band shape changes or position shifts are readily apparent between $\alpha^{\circ}(\tilde{\nu})$ and the total IR spectrum for the most intense bands. The band assignments are labeled in Fig. 1 and a detailed table of band positions in the pure liquids IR spectra obtained from AIMD simulations is provided in the Supplementary Material (see Table S1). As demonstrated previously for DMSO, the $\alpha^{\times}(\tilde{\nu})$ term is in fact negative in selected cases, most notably for δ_{CH_3} bending modes of the methyl group. The significance of this observation lies in discovering that the solvation environment can effectively suppress intramolecular modes of specific symmetry, thus precluding their experimental detection in the IR spectrum of the bulk liquid [35].

The magnitude of intermolecular cross-component correlations in the DMSO–GBL system is revealed in Fig. 2, where we lump together the intra- and intermolecular terms within the single component—i.e. $\alpha_1^{\circ}(\tilde{\nu}) + \alpha_1^{\times}(\tilde{\nu})$ for DMSO and $\alpha_2^{\circ}(\tilde{\nu}) + \alpha_2^{\times}(\tilde{\nu})$ for GBL, cf. Eq. 12—in order to clearly extract the contribution of the cross-component term, $\alpha_{12}^{\times}(\tilde{\nu})$. It turns out that $\alpha_{12}^{\times}(\tilde{\nu})$ is responsible for $\sim 15\%$ of the total IR intensity in the discussed spectral range. Its importance is particularly visible for the most intense IR bands. Another observation of great significance is that the liquids themselves respond at each other's vibrational frequencies, as clearly manifested by the non-zero intensity of the DMSO spectrum at the $\nu_{C_1=O_1}$ band of GBL and the complementary phenomenon observed in the GBL spectrum at the $\nu_{S=O}$ band of DMSO. We have previously observed such mutual polarization effects in IR spectra, even for monoatomic solutes that technically should be lacking any IR response within the mid-IR range, yet still show weak solvent bands in their contribution to the total IR spectrum, the magnitude of which depends on the solute's polarizability [36,52,72]. Notably, hydrated DMSO responds at the ν_{O-H} band

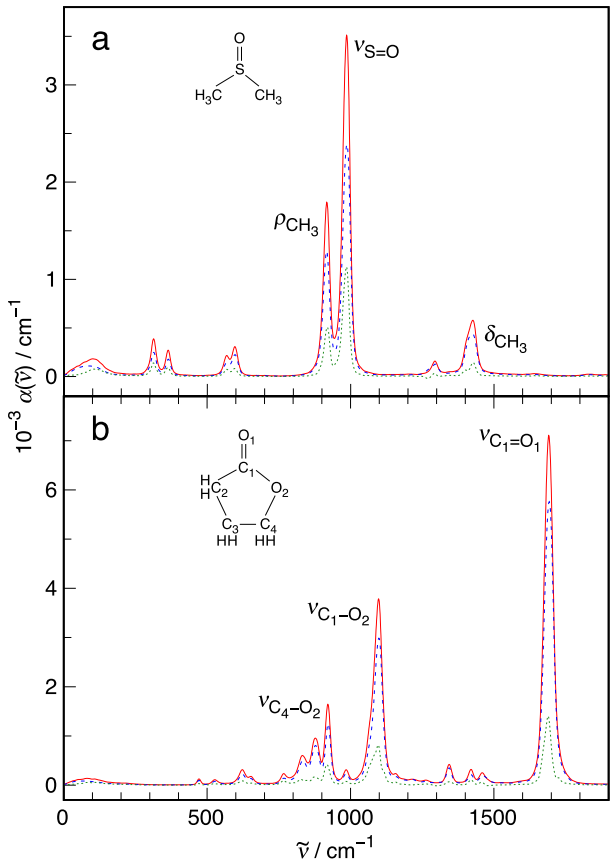

Fig. 1. IR spectrum of (a) pure liquid DMSO [35] and (b) pure liquid GBL [37] (red solid lines) decomposed into the intra- (blue dashed lines) and intermolecular (green dotted lines) terms. Insets show the molecular structures of the solvents and the atom numbering used in this work. The assignments of the most intense bands in the spectra are based on previous work [37,35]. (For interpretation of the references to colour in this figure legend, the reader is referred to the web version of this article.)

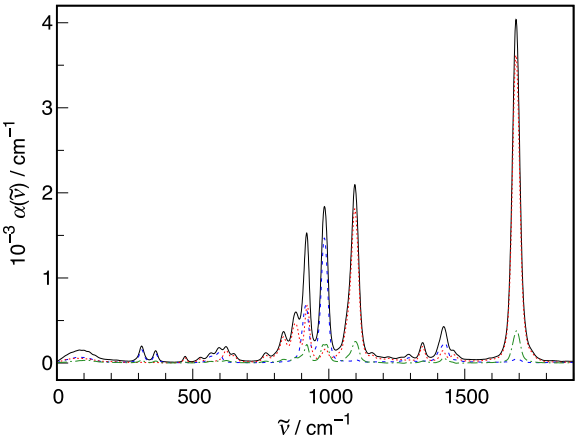

Fig. 2. IR spectrum of the DMSO–GBL system (black solid line) decomposed into DMSO (blue dashed line), GBL (red dotted line) and cross-component (green dashed-dotted line) contributions. (For interpretation of the references to colour in this figure legend, the reader is referred to the web version of this article.)

of water with band intensity as much as 50% of water itself as measured by molar absorptivity [73].

The validity of the reported spectra depends crucially on the adequate statistical sampling of the phase space of the system. Performing multiple independent simulations was found to be necessary to obtain reliable estimates of diffusion coefficients even for simple Lennard–Jones fluids [74]. As expected, this problem is further exacerbated by the short time scales available in AIMD simulations [75]. The importance of proper convergence of TCFs for producing reliable IR spectra was mentioned already in pioneering papers in the field [50,43,44]. The particular relevance of this convergence for the cross-correlation terms has been also well attested for over a decade [54]. The superior quality of the spectra obtained by averaging over independent trajectories (as in this work) is further demonstrated by analyzing the confidence interval of IR spectra and their components, as found in the Supplementary Material (see Figs. S2, S3).

The studied system is characterized by a distinct excess IR spectrum for the most intense bands, as shown in Fig. 3 together with the ideal spectrum, i.e. $(c_1^r\alpha_1^* + c_2^r\alpha_2^*)$ in Eq. (3). The shapes of the peaks observed in the excess spectrum are in agreement with the previously discussed model cases [21]. Namely, $\nu_{C_1=O_1}$ and $\nu_{S=O}$ bands show clear signs of band shifting with one positive and one negative excess peak. On the contrary, the $\nu_{C_1-O_2}$ band shows two negative peaks on both sides of a larger positive peak with the corresponding two zero-value points, indicative of a band broadening process, possibly coupled with a concomitant band shift. However, instead of just contending oneself with the qualitative description of the band changes upon the formation of a solution, thanks to the rigorous decomposition scheme outlined in Section 2.3 it is now possible to attribute them to distinct modifications of intra- and intermolecular IR response in solution vs the bulk liquids.

Focusing first on the intramolecular part of the IR spectrum (see Fig. 4), it is readily apparent that the $\Delta\alpha_i^\circ$ terms in Eq. (13) are already surprisingly good predictors of the shape of the total excess spectrum. Even not taking into the account the intermolecular correlations of molecular dipoles, the TCF of a single molecular dipole turns out to be a sensitive probe of the solvation environment as reflected by the changes in the intramolecular contribution to the IR spectrum. However, it is by itself not a perfect predictor of the entire excess spectrum, as clearly evidenced by the different character of the changes in the $\nu_{C_1-O_2}$ band of GBL at ~ 1100 cm^{-1} (cf. Fig. 3). Considering only the intramolecular contribution, the ester group vibrations of GBL as shown in Fig. 1 all show a clear redshift pattern in the partial excess spectrum with one positive and one negative peak. However, this redshift is very slight as will be discussed below and the excess spectrum clearly shows the "resolution enhancement" effect offered by the method [20]. On the other hand, only the most intense $\nu_{S=O}$ band of DMSO shows such features. Other bands, notably the ρ_{CH_3} and δ_{CH_3} vibrations, are characterized by simple decreasing intensity.

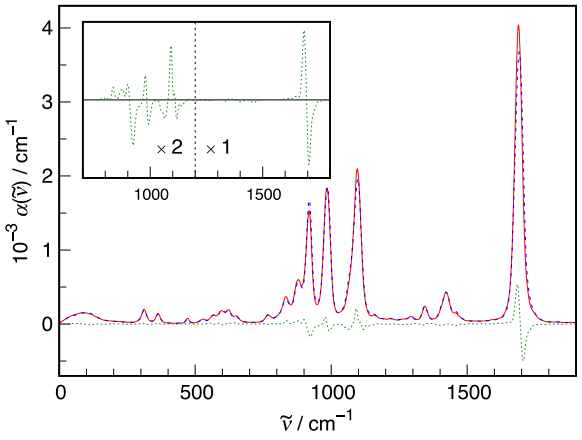

Fig. 3. IR spectrum of the DMSO–GBL system (red solid line) compared to the ideal spectrum of the same system (blue dashed line) and the corresponding excess IR spectrum (green dotted line). Inset shows a magnified view of the excess spectrum. (For interpretation of the references to colour in this figure legend, the reader is referred to the web version of this article.)

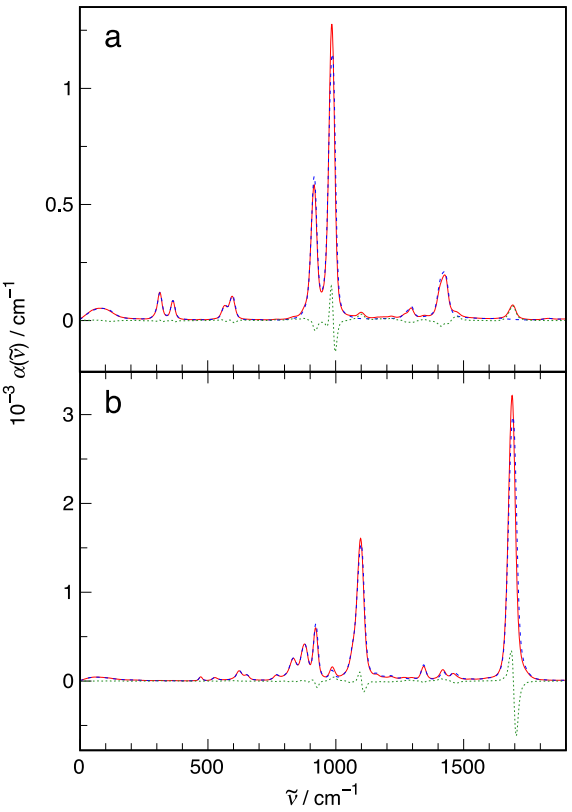

Fig. 4. The intramolecular terms due to (a) DMSO and (b) GBL in the IR spectrum of the DMSO–GBL system (red solid lines), the corresponding terms in the IR spectra of pure liquids scaled by relative concentrations (blue dashed lines) and the change of the intramolecular IR response of liquids in solution (green dotted lines). (For interpretation of the references to colour in this figure legend, the reader is referred to the web version of this article.)

Contrary to the intramolecular terms, the changes in the intermolecular part of the IR spectrum of the components (see Fig. 5) are marked by a pronounced intensity decrease, irrespective of the vibrational band. Comparing the solution vs the bulk liquid, however, it is also readily seen that the red shift of most of the strong bands is more apparent here than in the intramolecular term. The intensity decrease is most probably an effect of the intermolecular interactions within the component being partially substituted by interactions between the components of the solution, as corroborated by the undoubtedly positive contribution of the $\alpha_{12}^{\times}(\tilde{\nu})$ term, cf. Fig. 2.

In order to estimate the importance of the different terms in Eq. (13) on the computed excess spectrum, we show in Fig. 6 the contributions of the intra- and intermolecular terms combined for both solvents, as well as the cross-component contribution. As clearly seen in the Figure, the excess IR spectrum is not decisively shaped by any of the terms, but is a result of the interplay of intra- and intermolecular effects, none of which can be deemed negligible. As remarked above, the excess intramolecular IR spectrum of both solvents taken together, $\Delta\alpha_1^\circ + \Delta\alpha_2^\circ$, is a decent predictor of

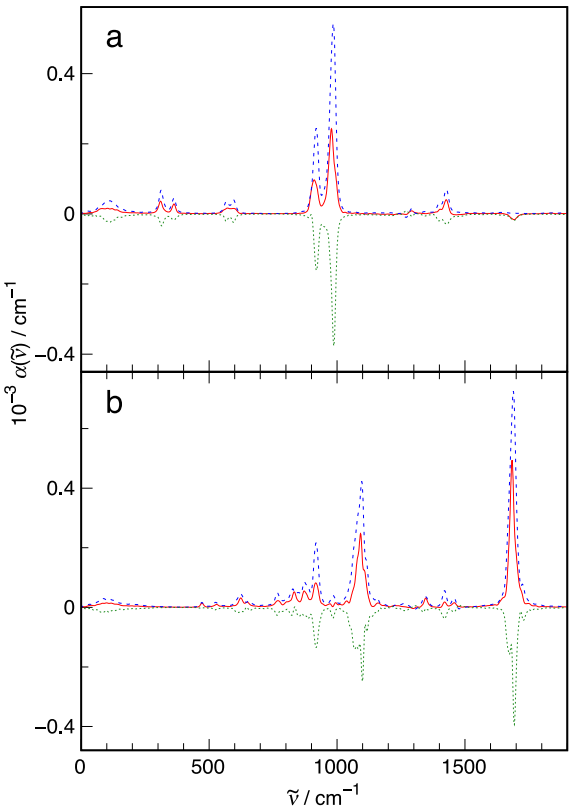

Fig. 5. The intermolecular terms within the component due to (a) DMSO and (b) GBL in the IR spectrum of the DMSO–GBL system (red solid lines), the corresponding terms in the IR spectra of pure liquids scaled by relative concentrations (blue dashed lines) and the change of the intermolecular IR response of liquids in solution (green dotted lines). (For interpretation of the references to colour in this figure legend, the reader is referred to the web version of this article.)

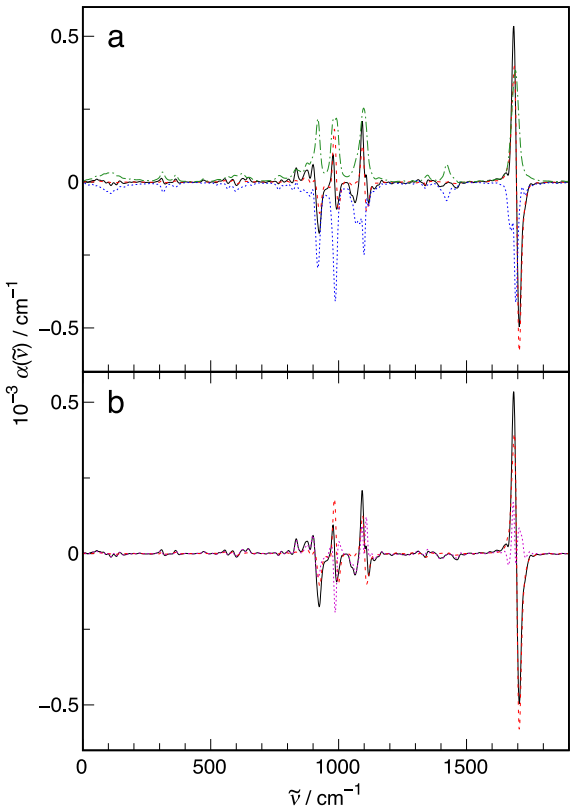

Fig. 6. (a) Excess IR spectrum of the DMSO–GBL system (black solid line) decomposed into the change of the intramolecular IR response of the components (red dashed line), the change of the intermolecular IR response of the components (blue dotted line) and the cross-component contribution (green dashed-dotted line). Part (b) shows the same spectra with the two latter terms grouped together (magenta dotted line). (For interpretation of the references to colour in this figure legend, the reader is referred to the web version of this article.)

the *shape* of the entire excess spectrum. On the other hand, the excess intermolecular IR spectrum, $\Delta\alpha_1^{\times} + \Delta\alpha_2^{\times}$, and the cross-component spectrum, $\alpha_{12}^{\times}$, provide the *modulation* of the excess IR response and are crucially important to predict its final shape.

The two latter terms indeed work in opposite directions as a result of the substitution of intermolecular interactions within the bulk liquid by likewise interactions between the two components of the mixture. Accordingly, they show a good deal of cancellation and—although their magnitude when considered separately is comparable to or even greater than that of the intramolecular excess spectrum—taken together they account for modulation that shapes the fine details of the excess IR spectrum. Fig. 6b, where the discussed terms are grouped together, clearly shows that the cancellation effect is incomplete and the distinct changes in cross-component vs internal intermolecular interactions play a decisive role in the total excess spectrum.

While the excess IR spectrum is strictly defined by the composition of the mixture, the affected spectrum is to a certain degree arbitrary, as the subtraction coefficients k_i in Eq. (6) must be obtained numerically based on some additional assumptions. There exists a strict lower bound for k below which the obtained affected spectrum becomes nonphysical (i.e., takes negative values at some spectral range). However, it can be strictly determined in a two-component system only by examining a vibrational band at which one of the components is active and the other one is transparent [21]. On the other hand, the upper bound for k cannot be determined precisely. Nevertheless, the band-fitting approach provides an accurate estimation of the bulk component contribution to the difference spectrum. The assumption of a too high fraction of the affected component of the system leads to a significant contribution of the bulk spectrum to the difference one, when the latter is represented as a sum of analytical bands and the bulk spectrum [14].

The same reasoning lies at the root of the spectral similarity method (SSM) [16,17], which is based on factor analysis algorithms developed by Malinowski [76–78]. Briefly, the series of trial spectra with varying k is decomposed into maximally orthogonal factors which are then compared to the bulk spectrum using a simple χ^2 metric. The analysis is performed for smaller subsets of trial spectra ("windows") of width W and plotting the sum of χ^2 values in the k–W plane reveals regions of high similarity (i.e., low $\sum\chi^2$ and significant bulk spectrum contribution) and low similarity (i.e., high $\sum\chi^2$ and negligible bulk spectrum contribution). The cutoff k value of the low similarity region in the $W \to 1$ window width limit (in practice $W \geqslant 3$ is required for the algorithm to work) is then treated as the upper bound of possible k values and serves as a reliable estimation of the affected component contribution to the IR spectrum of the mixture [16,17]. The SSM algorithm was already used by us in the analysis of computational IR spectra obtained on the basis of AIMD simulations [36,79].

The procedure of finding the mutually affected spectrum of both components in a two-component system should be performed independently for both substances, ideally using a spectral region transparent to one of the components in each case. In the studied DMSO–GBL system, this condition is fulfilled by the $\nu_{C_1=O_1}$ band of GBL, which is located in the region of vanishing absorption for DMSO. Therefore, it was selected for the application

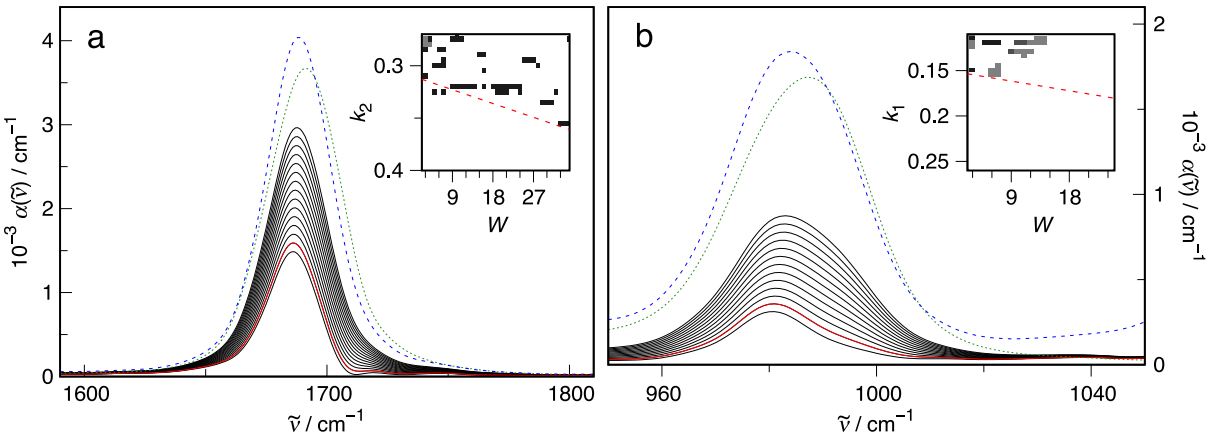

Fig. 7. (a) Spectral similarity-based determination of the affected GBL contribution in the DMSO–GBL system from the $\nu_{C_1=O_1}$ band of GBL: IR spectrum of the system (blue dashed line), IR spectrum of pure GBL scaled by relative concentration (green dotted line), the subtracted trial spectra, $\alpha_m - (1-k_2)c_2^r\alpha_2^*$, for $k_2 = 0.28$–0.7 in 0.03 steps (thin black lines) and the final affected GBL spectrum for $k_2 = 0.31$, α_{GBL}^A (red solid line). (b) The respective determination of the affected DMSO contribution in the DMSO–GBL system from the $\nu_{S=O}$ band of DMSO after subtracting the contribution of bulk GBL with $k_2 = 0.31$: corrected IR spectrum of the system (blue dashed line), IR spectrum of pure DMSO scaled by relative concentration (green dotted line), the subtracted trial spectra, $\alpha_{GBL}^A - (1-k_1)c_1^r\alpha_1^*$, for $k_1 = 0.12$–0.48 in 0.03 steps (thin black lines) and the final affected DMSO spectrum for $k_1 = 0.15$ (red solid line). Insets show the respective spectral similarity maps using window width W, where white regions indicate high similarity to bulk spectrum and darker shades indicate lowering similarity. Red dashed lines indicate the cutoff for the lower similarity regions. (For interpretation of the references to colour in this figure legend, the reader is referred to the web version of this article.)

of SSM in order to determine the k_2 subtraction coefficient for GBL. The results of this SSM analysis are shown in Fig. 7a. The trial series of subtracted spectra was generated by varying the k_2 subtraction factor from 0.27 (the absolute lower bound below which the GBL spectrum in the $\nu_{C_1=O_1}$ range becomes negative) up to 0.7 in 0.005 steps. The analysis by SSM unambiguously points to $k_2 = 0.31$ as the upper bound in the $W \to 1$ limit, above which the bulk GBL contribution becomes substantial (as measured by the $\sum\chi^2$ similarity metric). As seen in Fig. 7a, the spectrum of affected GBL is slightly red-shifted with respect to the bulk solvent, as expected based on the mixture spectrum and predicted by a positive feature of the excess spectrum (cf. Fig. 3). This indicates increased polarization of the C_1=O_1 bond, possibly due to the influence of favorable intermolecular interactions.

The requirement of transparency of a selected spectral region to the other component in a two-component system is not strictly fulfilled by DMSO, as GBL is spectrally active in the $\nu_{S=O}$ range (cf. Fig. 2). However, the contribution from DMSO is clearly dominant and, furthermore, the subtraction of bulk GBL spectrum with the selected k_2 factor further diminishes the IR absorption from GBL. Therefore, the $\nu_{S=O}$ range was used for SSM analysis of the mixture spectrum after the removal of bulk GBL contribution, i.e., $\alpha_{GBL}^A = \alpha_m - (1-k_2)c_2^r\alpha_2^*$, in order to determine the k_1 subtraction factor for DMSO. The results of the SSM analysis are summarized in Fig. 7b. This time, the trial series of subtracted spectra was generated by varying the k_1 subtraction factor from 0.11 (the lower bound below which the IR spectrum in the $\nu_{S=O}$ range becomes negative) up to 0.5 in 0.005 steps. The analysis by SSM unequivocally indicates $k_1 = 0.15$ as the upper bound in the $W \to 1$ limit, above which the bulk DMSO contribution becomes significant when measured by the $\sum\chi^2$ metric. As seen in Fig. 7b, the spectrum of affected DMSO is also slightly red-shifted with respect to bulk DMSO, again as expected based on the positive feature of the excess spectrum (cf. Fig. 3). Therefore, the S=O bond—which is already significantly polarized in the bulk liquid [35]—becomes further polarized in the mixture with GBL, further supporting generally favorable intermolecular interactions.

The final affected spectrum with respect to both solvents, obtained from Eq. 6 using the determined values of the k_1 and k_2 subtraction factors, is shown in Fig. 8. It is readily apparent that the affected spectrum is particularly pronounced in the 800–1800 cm^{-1} range, where the more polarizable bonds are vibrationally active, notably for the $\nu_{C_1=O_1}$, $\nu_{C_1-O_2}$, $\nu_{S=O}$ and $\nu_{C_4-O_2}$ bands (cf. Fig. 1). All the mentioned bands are characterized by clear red shift with respect to the ideal spectrum, i.e., the pure solvents band positions. On the contrary, the low frequency part of the IR spectrum below 800 cm^{-1} is characterized both by the insignificant excess spectrum and the very small intensity of the affected spectrum, suggestive of the near ideal character of the mixture in this particular range.

Following the decomposition scheme laid out in Eq. (14), the affected spectrum of the system can be rigorously represented as the sum of the changes in the intra- and intermolecular parts of the spectrum, as well as the cross-component contribution. Similar to the presentation in Fig. 6 for the excess spectrum, Fig. 9 illustrates the outcome of such decomposition for α^A. The most apparent difference with respect to the excess spectrum is that the change of the intramolecular part of IR absorption is almost always positive in the affected spectrum in the studied spectral range. This is of course related to the presence of subtraction factors $k_{1,2}$ in Eq. 6. Furthermore, since the cross-component term $\alpha_{12}^{\times}$ is the same as

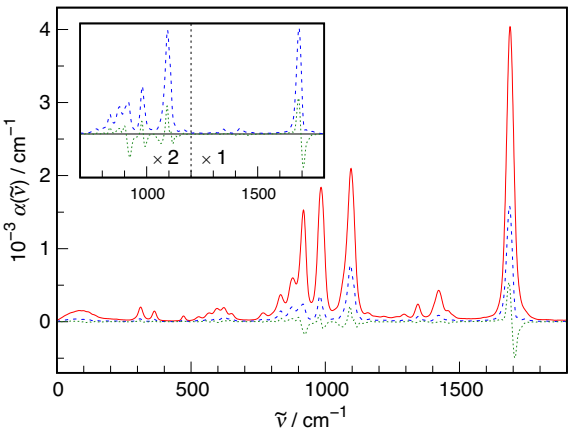

Fig. 8. IR spectrum of the DMSO–GBL system (red solid line), the corresponding affected spectrum (blue dashed line) and the excess IR spectrum (green dotted line). Inset shows a magnified view of the affected and excess spectra.

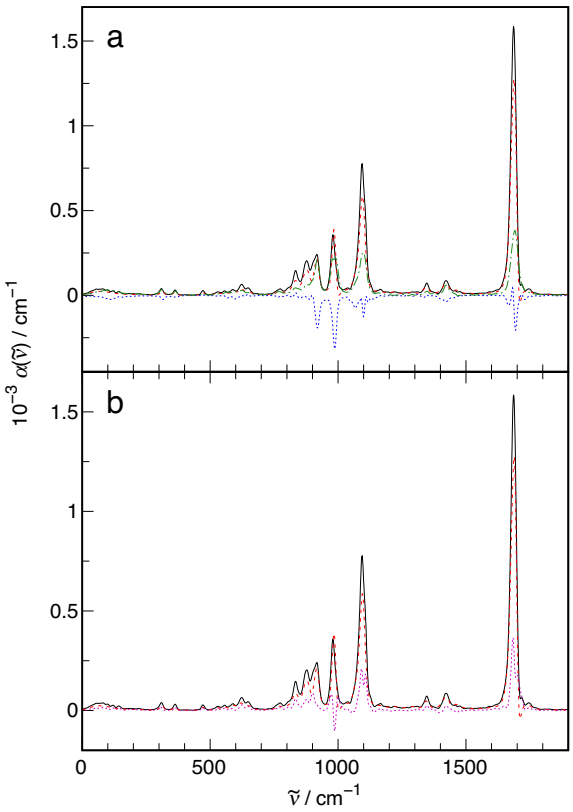

Fig. 9. (a) Affected spectrum of the DMSO–GBL system (black solid line) decomposed into the change of the intramolecular IR response of the components (red dashed line), the change of the intermolecular IR response of the components (blue dotted line) and the cross-component contribution (green dashed-dotted line). Part (b) shows the same spectra with the two latter terms grouped together (magenta dotted line). (For interpretation of the references to colour in this figure legend, the reader is referred to the web version of this article.)

in the excess spectrum, while the intermolecular terms within a single component are scaled by subtraction factors $k_{1,2}$, their apparent cancellation is much less pronounced than in the excess spectrum (cf. Fig. 6). Again, the final appearance of the affected spectrum is determined by the interplay of intra- and intermolecular effects, the latter acting both within the components and between them. The intramolecular part of the affected spectrum is once more found to predict the *shape* of the entire spectrum. However, the fine *modulation* of this shape by all the intermolecular terms grouped together is even more pronounced than in the case of excess IR spectrum due to the virtual absence of the cancellation effect.

We further note that the ratio $k_1 : k_2 \approx 1 : 2$ is indicative of the most probable intermolecular complex in the DMSO–GBL system at $x_1 = 0.5$. In a two-component system, determination of the affected spectra in a broad composition range can lead to the ascription of the most represented intermolecular complexes at different concentration regimes [9]. In this particular case, the DMSO · 2 GBL complex seems to be the dominant intermolecular arrangement in the studied system. The most possible explanation for the binding type in such complexes is of course the C–H…O hydrogen bonding, which is one of the dominant intermolecular interactions in liquid DMSO [35]. In the Supplementary Material, we provide a snapshot of an instantaneous structure of a DMSO · 2 GBL complex as found in AIMD trajectory, held together by two C–H…O hydrogen bonds donated by GBL molecules to the DMSO oxygen atom (see Fig. S4). Their length (∼ 3.32 Å) is well within

Table 1
The position at maximum ($\tilde{\nu}$/cm^{-1}) of the most prominent vibrational bands of DMSO and GBL in the IR spectrum of the mixture, the excess IR spectrum, the affected spectrum and the discussed intra- and intermolecular spectral contributions

Spectrum type	$\nu_{S=O}$	$\nu_{C_1=O_1}$
α_m	984	1688
α°	985	1690
$\alpha^{\times}$	978	1684
$\alpha^{\times}_{12}$	980	1691
α^{*}	986	1691
$\alpha^{\circ,*}$	987	1693
$\alpha^{\times,*}$	985	1689
α^{A}	980	1686
α^{E}_{+} [a]	978	1684
α^{E}_{-} [b]	992	1706

[a] The positive peak in the excess IR spectrum.
[b] The negative peak in the excess IR spectrum.

the attractive potential energy surface basin for C–H…O contacts in liquid DMSO [35].

Finally, it is instructive to compare the band parameters of the affected vs excess spectrum and also identify, which of the factors in Eq. (13) are primarily responsible for the band shifts observed in the IR spectrum of the mixture with respect to pure components. The results for band positions at maximum are summarized in Table 1.

Starting from the IR spectrum of the mixture, α_m, both analyzed bands are red-shifted with respect to the pure components spectra, $\alpha^{*}_{1,2}$, by −2 and −3 cm^{-1} for $\nu_{S=O}$ and $\nu_{C_1=O_1}$, respectively. Notably, the effect is more pronounced in the $\alpha^{\times}_{1,2}$ contribution than in the corresponding self terms, $\alpha^{\circ}_{1,2}$. The latter observation is also valid for pure components spectra, where the cross terms, $\alpha^{\times,*}_{1,2}$, and the self terms, $\alpha^{\circ,*}_{1,2}$ are red- and blue shifted, respectively, comparing to the entire IR spectra of pure DMSO and GBL. It is worth stressing that intermolecular contributions in general reflect the polarization effects in the liquid phase more than the intramolecular ones, as already found in the pioneering study of liquid water [54].

The positive part of excess IR spectrum is characterized by the most pronounced red shift for the two discussed bands. A seen in Table 1, it shares these band positions with the $\alpha^{\times}_{1,2}$ intermolecular contribution in the IR spectrum of the mixture. Thus, the excess IR spectrum seems to be driven mainly by the dramatic changes in the intermolecular contribution within a component that are not fully balanced by the emerging cross-component part of the spectrum. Finally, the affected spectrum determined with the SSM method shows band positions that are very close to the positive peaks noted in the excess IR spectrum. Consequently, the latter can serve as a valuable predictor of the band positions in the affected spectrum. Furthermore, excess IR spectrum has the advantage of being assumption-free and thus rigorously defined. The observed correspondence between the positive peaks in the excess spectrum and the band positions in the affected spectrum can possibly serve as a guide in the semi-automatic methods of affected spectra determination.

5. Conclusions

The study of various excess thermodynamic functions is one of the fundamental tasks in physical chemistry of solutions. Excess IR spectroscopy, extending the applicability of this useful approach, delivers a rigorously defined picture of the deviations of the IR spectrum of a mixture from the case of an ideal solution for which an additivity assumption holds. Somewhat surprisingly, although tremendously useful, excess IR spectroscopy has been poorly studied from a computational perspective. In this contribution, the con-

cept of excess IR spectra is analyzed from linear response theory owing to the availability of time evolution of molecular dipoles in ab initio molecular dynamics simulations. The decomposition of the total dipole moment of the system into individual molecular contributions allows for an unambiguous partitioning of the IR spectrum of a liquid into an intra- and intermolecular part. The extension to two-component systems introduced in this work adds the cross-component correlation (the mutual interaction spectrum) to this picture. By subtracting decomposed spectra of pure liquids from the decomposed spectrum of the mixture, the excess IR spectrum is found to be an algebraic sum of the changes in the intra- and intermolecular parts of the spectra of both components and the mutual interaction spectrum. This allows for a profound insight into the mechanisms underlying the experimentally determined excess IR spectrum and the deeper discussion of changes in intramolecular interactions accompanying the mixing of the liquids.

The introduced methodology is thoroughly tested on the example of an equimolar mixture of two important industrial solvents, dimethyl sulfoxide and γ-butyrolactone, for which IR spectra are obtained entirely from AIMD simulations, without resorting to experimental input. The studied system is characterized by a distinct excess IR spectrum, particularly pronounced for the more polarizable bonds connected with intense IR absorption. It is found that while the excess intramolecular IR spectrum is a decent predictor of the *shape* of the entire excess spectrum, the excess intermolecular spectrum and the cross-component spectrum provide the non-negligible *modulation* of the excess IR response and are crucially important for the prediction of its final shape. The two latter contributions act in opposite directions, but due to the changes in intermolecular interactions between the pure liquids and the solution owing to the non-ideality of the studied system, their apparent cancellation is imperfect and, taken together, they have a decisive role in the observed IR band shifts in the mixture with respect to the pure components.

One of the drawbacks of excess molar absorption coefficients is that they do not represent physical observable quantities, since excess spectra may contain negative features. On the other hand, the difference spectra method seeks to obtain the so-called affected spectra by numerically subtracting the bulk component contribution until only the IR spectrum of the spectrally affected component is effectively isolated. The affected IR spectrum of both components treated on equal terms, i.e., without the solute–solvent distinction, is obtained here chemometrically by applying the spectral similarity method. Furthermore, an exact mathematical relationship between the affected and excess IR spectrum is derived. Thus, the affected spectrum can be decomposed in the same manner as the excess one and analyzed from the point of view of changes in the intra- and intermolecular contributions of the components, with the cross-component contribution exactly the same as in excess spectrum. The latter fact leads to a reduced cancellation effect in the intermolecular contributions in the affected spectrum, making it a physically justified counterpart of the excess IR spectrum that provided a complementary view of the interactions in the mixture. Excess IR spectrum is also discovered as an accurate predictor of the band shifts in the affected spectrum. Based on the simplicity and unambiguous way of calculating the excess spectrum, it can possibly serve as a guidance in the semi-automatic methods of affected spectra determination.

Declaration of Competing Interest

The authors declare that they have no known competing financial interests or personal relationships that could have appeared to influence the work reported in this paper.

Acknowledgments

This work was supported by the statutory fund of Gdańsk University of Technology. Calculations were performed at the Academic Computer Center in Gdańsk (TASK). I thank Piotr Bruździak for valuable discussions about the spectral similarity method and chemometric analysis of IR spectra.

Appendix A. Supplementary material

Supplementary data associated with this article can be found, in the online version, at https://doi.org/10.1016/j.molliq.2021.117544.

References

[1] S. Bratos, R.M. Pick (Eds.), Vibrational Spectroscopy of Molecular Liquids and Solids, NATO ASI Series B: Physics, Vol. 56, Springer, US, New York, 1980.
[2] M.C.R. Symons, Structure in solvents and solutions–NMR and vibrational spectroscopic studies, Chem. Soc. Rev. 12 (1983) 1–34.
[3] J.M. Chalmers, Mid-infrared spectroscopy of the condensed phase, in: P. Griffiths, J.M. Chalmers (Eds.), Handbook of Vibrational Spectroscopy, John Wiley & Sons Ltd, Chichester, 2002, pp. 128–140.
[4] M.A. Czarnecki, Y. Morisawa, Y. Futami, Y. Ozaki, Advances in Molecular Structure and Interaction Studies Using Near-Infrared Spectroscopy, Chem. Rev. 115 (2015) 9707–9744.
[5] J. Stangret, E. Kamieńska-Piotrowicz, J. Szymańska-Cybulska, Analysis of spectral data by complementary methods. Inspection of the molecular complex in N, N-dimethylformamide–methanol mixtures, Spectrochim. Acta A 61 (2005) 3043–3050.
[6] J. Stangret, E. Kamieńska-Piotrowicz, J. Szymańska-Cybulska, FT-IR studies of molecular interactions in formamide–methanol mixtures, Vib. Spectrosc. 44 (2007) 324–330.
[7] J.-J. Max, C. Chapados, Infrared spectroscopy of acetone-hexane liquid mixtures, J. Chem. Phys. 126 (2007) 154511.
[8] J.-J. Max, C. Chapados, Infrared spectroscopy of methanol-hexane liquid mixtures. II. The strength of hydrogen bonding, J. Chem. Phys. 130 (2009) 124513.
[9] M. Śmiechowski, Vibrational spectroscopic studies of N, N'-dimethylpropyleneurea–water system: Affected solvent spectra and factor analysis, Spectrochim. Acta A 79 (2011) 712–721.
[10] R. Balaji, M.G. Sankar, M.C. Sekhar, M.C. Shekar, FT-IR Spectroscopic study of excess thermodynamic properties of liquid mixtures containing N-methylformamide with 2-alkoxyethanols at various temperatures, J. Mol. Liquids 216 (2016) 330–341.
[11] H.-J. van Manen, J. Gerretzen, M. Smout, G. Postma, J.J. Jansen, Quantitative vibrational spectroscopy on liquid mixtures: concentration units matter, Analyst 146 (2021) 3150–3156.
[12] O. Kristiansson, J. Lindgren, J. de Villepin, A quantitative infrared spectroscopic method for the study of the hydration of ions in aqueous solutions, J. Phys. Chem. 92 (1988) 2680–2685.
[13] J. Stangret, Solute-affected vibrational spectra of water in Ca(ClO4)2 aqueous solutions, Spectrosc. Lett. 21 (1988) 369–381.
[14] J. Stangret, T. Gampe, Hydration sphere of tetrabutylammonium cation. FTIR studies of HDO spectra, J. Phys. Chem. B 103 (1999) 3778–3783.
[15] M. Śmiechowski, J. Stangret, Vibrational spectroscopy of semiheavy water (HDO) as a probe of solute hydration, Pure Appl. Chem. 82 (2010) 1869–1887.
[16] P. Bruździak, A. Panuszko, J. Stangret, Chemometric determination of solute-affected solvent vibrational spectra as a superior way of information extraction on solute solvation phenomena, Vib. Spectrosc. 54 (2010) 65–71.
[17] P. Bruździak, P.W. Rakowska, J. Stangret, Chemometric Method of Spectra Analysis Leading to Isolation of Lysozyme and CtDNA Spectra Affected by Osmolytes, Appl. Spectrosc. 66 (2012) 1302–1310.
[18] R. Nieto, M.C. González, F. Herrero, Thermodynamics of mixtures: Functions of mixing and excess functions, Am. J. Phys. 67 (1999) 1096–1099.
[19] Q. Li, G. Wu, Z. Yu, The Role of Methyl Groups in the Formation of Hydrogen Bond in DMSO–Methanol Mixtures, J. Am. Chem. Soc. 128 (2006) 1438–1439.
[20] Q. Li, N. Wang, Q. Zhou, S.Q. Sun, Z. Yu, Excess Infrared Absorption Spectroscopy and Its Applications in the Studies of Hydrogen Bonds in Alcohol-Containing Binary Mixtures, Appl. Spectrosc. 62 (2008) 166–170.
[21] Y. Zhou, Y.-Z. Zheng, H.-Y. Sun, G. Deng, Z.-W. Yu, Two-State or Non-Two-State? An Excess Spectroscopy-based Approach to Differentiate the Existing Forms of Molecules in Liquids Mixtures, Sci. Rep. 5 (2015) 16379.
[22] Y. Zhou, J. Xu, N.-N. Wang, Z.-W. Yu, Excess Spectroscopy: Concept and Applications, Acta Phys.-Chim. Sin. 32 (2016) 239–248.
[23] Y. Zhang, Z. Wu, Y. Wang, H. He, Z. Yu, Excess spectroscopy and its applications in the study of solution chemistry, Pure Appl. Chem. 92 (2020) 1611–1626.
[24] Y. Koga, F. Sebe, T. Minami, K. Otake, K.-I. Saitow, K. Nishikawa, Spectrum of Excess Partial Molar Absorptivity. I. Near Infrared Spectroscopic Study of Aqueous Acetonitrile and Acetone, J. Phys. Chem. B 113 (2009) 11928–11935.

[25] F. Sebe, K. Nishikawa, Y. Koga, Spectrum of excess partial molar absorptivity. Part II: a near infrared spectroscopic study of aqueous Na-halides, Phys. Chem. Chem. Phys. 14 (2012) 4433–4439.
[26] F. Sebe, K. Nishikawa, Y. Koga, Spectra of excess molar absorptivity of aqueous solutions of ionic liquids: Universal chromophores for aqueous electrolytes?, J Mol. Liquids 238 (2017) 570–573.
[27] D. Marx, J. Hutter, Ab Initio Molecular Dynamics, Cambridge University Press, Cambridge, 2009.
[28] B. Kirchner, Theory of complicated liquids. Investigation of liquids, solvents and solvent effects with modern theoretical methods, Phys. Rep. 440 (2007) 1–111.
[29] B. Kirchner, P.J. di Dio, J. Hutter, Real-World Predictions from Ab Initio Molecular Dynamics Simulations, in: B. Kirchner, J. Vrabec (Eds.), Multiscale Molecular Methods in Applied Chemistry, Springer, Berlin, Heidelberg, 2012, pp. 109–153.
[30] A.A. Hassanali, J. Cuny, V. Verdolino, M. Parrinello, Aqueous solutions: state of the art in ab initio molecular dynamics, Philos. Trans. R. Soc. A 372 (2014) 20120482.
[31] K.H. Wujcik, T.A. Pascal, C.D. Pemmaraju, D. Devaux, W.C. Stolte, N.P. Balsara, D. Prendergast, Characterization of Polysulfide Radicals Present in an Ether-Based Electrolyte of a Lithium-Sulfur Battery During Initial Discharge Using In Situ X-Ray Absorption Spectroscopy Experiments and First-Principles Calculations, Adv. Energy Mater. 5 (2015) 1500285.
[32] M. Callsen, K. Sodeyama, Z. Futera, Y. Tateyama, I. Hamada, The Solvation Structure of Lithium Ions in an Ether Based Electrolyte Solution from First-Principles Molecular Dynamics, J. Phys. Chem. B 121 (2017) 180–188.
[33] C.C. Wang, J.Y. Tan, L.H. Liu, Ab initio molecular dynamics study of temperature and pressure-dependent infrared dielectric functions of liquid methanol, AIP Adv. 7 (2017) 035115.
[34] A. Korotkevich, D.S. Firaha, A.A.H. Padua, B. Kirchner, Ab initio molecular dynamics simulations of SO_2 solvation in choline chloride/glycerol deep eutectic solvent, Fluid Phase Equil. 448 (2017) 59–68.
[35] M. Śmiechowski, The influence of intermolecular correlations on the infrared spectrum of liquid dimethyl sulfoxide, Spectrochim. Acta A 260 (2021) 119869.
[36] M. Śmiechowski, J. Krakowiak, P. Bruździak, J. Stangret, Unique Agreement of Experimental and Computational Infrared Spectroscopy: a Case Study of Lithium Bromide Solvation in an Important Electrochemical Solvent, Phys. Chem. Chem. Phys. 19 (2017) 9270–9280.
[37] M. Śmiechowski, Visualizing spatially decomposed intermolecular correlations in the infrared spectra of aprotic liquids, J. Mol. Graph. 78 (2017) 148–157.
[38] J. Ingenmey, S. Gehrke, B. Kirchner, How to Harvest Grotthuss Diffusion in Protic Ionic Liquid Electrolyte Systems, ChemSusChem 11 (2018) 1900–1910.
[39] P.L. Silvestrelli, N. Marzari, D. Vanderbilt, M. Parrinello, Maximally-Localized Wannier Functions For Disordered Systems: Application To Amorphous Silicon, Solid State Commun. 107 (1998) 7–11.
[40] M. Thomas, M. Brehm, B. Kirchner, Voronoi dipole moments for the simulation of bulk phase vibrational spectra, Phys. Chem. Chem. Phys. 17 (2015) 3207–3213.
[41] P.L. Silvestrelli, M. Parrinello, Structural, electronic, and bonding properties of liquid water from first principles, J. Chem. Phys. 111 (1999) 3572–3580.
[42] M.-P. Gaigeot, M. Sprik, Ab Initio Molecular Dynamics Computation of the Infrared Spectrum of Aqueous Uracil, J. Phys. Chem. B 107 (2003) 10344–10358.
[43] R. Iftimie, M.E. Tuckerman, Decomposing total IR spectra of aqueous systems into solute and solvent contributions: A computational approach using maximally localized Wannier orbitals, J. Chem. Phys. 122 (2005) 214508.
[44] M.-P. Gaigeot, M. Martinez, R. Vuilleumier, Infrared spectroscopy in the gas and liquid phase from first principle molecular dynamics simulations: application to small peptides, Mol. Phys. 105 (2007) 2857–2878.
[45] J. Krakowiak, M. Śmiechowski, Excess molar volume and viscosity deviation for binary mixtures of γ-butyrolactone with dimethyl sulfoxide, J. Chem. Thermodyn. 110 (2017) 57–64.
[46] N.J. Jeon, J.H. Noh, Y.C. Kim, W.S. Yang, S. Ryu, S.I. Seok, Solvent engineering for high-performance inorganic–organic hybrid perovskite solar cells, Nat. Mater. 13 (2014) 897–903.
[47] N.J. Jeon, J.H. Noh, W.S. Yang, Y.C. Kim, S. Ryu, J. Seo, S.I. Seok, Compositional engineering of perovskite materials for high-performance solar cells, Nature 517 (2015) 476–480.
[48] N.G. Park, Methodologies for high efficiency perovskite solar cells, Nano Converg. 3 (2016) 15.
[49] D.A. McQuarrie, Statistical Mechanics, Harper & Row, New York, 1976.
[50] R. Ramírez, T. López-Ciudad, P. Kumar, D. Marx, Quantum corrections to classical time-correlation functions: Hydrogen bonding and anharmonic floppy modes, J. Chem. Phys. 121 (2004) 3973–3983.
[51] M. Thomas, M. Brehm, R. Fligg, P. Vöhringer, B. Kirchner, Computing vibrational spectra from ab initio molecular dynamics, Phys. Chem. Chem. Phys. 15 (2013) 6608–6622.
[52] M. Śmiechowski, J. Sun, H. Forbert, D. Marx, Solvation shell resolved THz spectra of simple aqua ions – distinct distance- and frequency-dependent contributions of solvation shells, Phys. Chem. Chem. Phys. 17 (2015) 8323–8329.
[53] J. Stangret, T. Gampe, Hydration of tetrahydrofuran derived from FTIR spectroscopy, J. Mol. Struct. 734 (2005) 183–190.
[54] M. Heyden, J. Sun, S. Funkner, G. Mathias, H. Forbert, M. Havenith, D. Marx, Dissecting the THz spectrum of liquid water from first principles via correlations in time and space, Proc. Natl. Acad. Sci. U.S.A. 107 (2010) 12068–12073.
[55] L. Martínez, R. Andrade, E.G. Birgin, J.M. Martínez, Packmol: A package for building initial configurations for molecular dynamics simulations, J. Comput. Chem. 30 (2009) 2157–2164.
[56] The cp2k Developers Group, cp2k v. 2.7, http://www.cp2k.org/ (2001–2015).
[57] J. Hutter, M. Iannuzzi, F. Schiffmann, J. VandeVondele, cp2k: atomistic simulations of condensed matter systems, WIREs Comput. Mol. Sci. 4 (2014) 15–25.
[58] J. VandeVondele, M. Krack, F. Mohamed, M. Parrinello, T. Chassaing, J. Hutter, Quickstep: Fast and accurate density functional calculations using a mixed Gaussian and plane waves approach, Comp. Phys. Commun. 167 (2005) 103–128.
[59] A.D. Becke, Density-functional exchange-energy approximation with correct asymptotic behavior, Phys. Rev. A 38 (1988) 3098–3100.
[60] C. Lee, W. Yang, R.G. Parr, Development of the Colle-Salvetti correlation-energy formula into a functional of the electron density, Phys. Rev. B 37 (1988) 785–789.
[61] S. Grimme, J. Antony, S. Ehrlich, H. Krieg, A consistent and accurate ab initio parametrization of density functional dispersion correction (DFT-D) for the 94 elements H-Pu, J. Chem. Phys. 132 (2010) 154104.
[62] S. Goedecker, M. Teter, J. Hutter, Separable dual-space Gaussian pseudopotentials, Phys. Rev. B 54 (1996) 1703–1710.
[63] G.J. Martyna, M.L. Klein, M. Tuckerman, Nosé-Hoover chains: The canonical ensemble via continuous dynamics, J. Chem. Phys. 97 (1992) 2635–2643.
[64] J. VandeVondele, F. Mohamed, M. Krack, J. Hutter, M. Sprik, M. Parrinello, The influence of temperature and density functional models in ab initio molecular dynamics simulation of liquid water, J. Chem. Phys. 122 (2005) 014515.
[65] E. Schwegler, J.C. Grossman, F. Gygi, G. Galli, Towards an assessment of the accuracy of density functional theory for first principles simulations of water. II, J. Chem. Phys. 121 (2004) 5400–5409.
[66] S. Yoo, X.C. Zeng, S.S. Xantheas, On the phase diagram of water with density functional theory potentials: The melting temperature of ice Ih with the Perdew–Burke–Ernzerhof and Becke–Lee–Yang–Parr functionals, J. Chem. Phys. 130 (2009) 221102.
[67] I.-F.W. Kuo, C.J. Mundy, M.J. McGrath, J.I. Siepmann, J. VandeVondele, M. Sprik, J. Hutter, B. Chen, M.L. Klein, F. Mohamed, M. Krack, M. Parrinello, Liquid Water from First Principles: Investigation of Different Sampling Approaches, J. Phys. Chem. B 108 (2004) 12990–12998.
[68] Y. Aihara, K. Sugimoto, W.S. Price, K. Hayamizu, Ionic conduction and self-diffusion near infinitesimal concentration in lithium salt-organic solvent electrolytes, J. Chem. Phys. 113 (2000) 1981–1991.
[69] M. Holz, S.R. Heil, A. Sacco, Temperature-dependent self-diffusion coefficients of water and six selected molecular liquids for calibration in accurate ^{1}H NMR PFG measurements, Phys. Chem. Chem. Phys. 2 (2000) 4740–4742.
[70] M. Tuckerman, Statistical Mechanics: Theory and Molecular Simulation, Oxford University Press, New York, 2010.
[71] S.A. Markarian, A.M. Terzyan, Surface Tension and Refractive Index of Dialkylsulfoxide + Water Mixtures at Several Temperatures, J. Chem. Eng. Data 52 (2007) 1704–1709.
[72] M. Śmiechowski, H. Forbert, D. Marx, Spatial decomposition and assignment of infrared spectra of simple ions in water from mid-infrared to THz frequencies: Li^+(aq) and F^-(aq), J. Chem. Phys. 139 (2013) 014506.
[73] A. Panuszko, P. Bruździak, M. Śmiechowski, M. Stasiulewicz, J. Stefaniak, J. Stangret, DMSO hydration redefined: Unraveling the hydrophobic hydration of solutes with a mixed hydrophilic–hydrophobic characteristic, J. Mol. Liquids 294 (2019) 111661.
[74] G. Pranami, M.H. Lamm, Estimating Error in Diffusion Coefficients Derived from Molecular Dynamics Simulations, J. Chem. Theory Comput. 11 (2015) 4586–4592.
[75] W. Dawson, F. Gygi, Equilibration and analysis of first-principles molecular dynamics simulations of water, J. Chem. Phys. 148 (2018) 124501.
[76] E.R. Malinowski, Factor Analysis in Chemistry, 3rd edn., Wiley, New York, 2002.
[77] K.J. Schostack, E.R. Malinowski, Preferred set selection by iterative key set factor analysis, Chemom. Intell. Lab. Syst. 6 (1989) 21–29.
[78] E.R. Malinowski, Obtaining the key set of typical vectors by factor analysis and subsequent isolation of component spectra, Anal. Chim. Acta 134 (1982) 129–137.
[79] M. Śmiechowski, Unusual Influence of the Fluorinated Anions on the Stretching Vibrations of Liquid Water, J. Phys. Chem. B 122 (2018) 3141–3152.